DOI: 10.31276/VJSTE.66(1).10-15

Effect of annealing temperature and doping concentrations on structure and optical properties of Eu^{3+}-doped TiO_2 nanomaterials

Nguyen Tri Tuan[1*], Tong Thi Hao Tam[2*], Nguyen Tu[3], Do Quang Trung[3], Nguyen Van Du[3], Tran Minh Tien[3], Vu Thi Hang[1], Nguyen Trong Tuan[1], Nguyen Van Quang[4], Manh Trung Tran[5]

[1]*College of Natural Sciences, Can Tho University, Campus II, 3/2 Street, Xuan Khanh Ward, Ninh Kieu District, Can Tho City, Vietnam*
[2]*School of Information Technology and Digital Economics, National Economics University, 207 Giai Phong Street, Dong Tam Ward, Hai Ba Trung District, Hanoi, Vietnam*
[3]*Faculty of Fundamental Sciences, Phenikaa University, Yen Nghia Ward, Ha Dong District, Hanoi, Vietnam*
[4]*Department of Chemistry, Hanoi Pedagogical University 2, Nguyen Van Linh Street, Xuan Hoa Ward, Phuc Yen City, Vinh Phuc Province, Vietnam*
[5]*Faculty of Materials Science and Engineering, Phenikaa University, Yen Nghia Ward, Ha Dong District, Hanoi, Vietnam*

Received 9 March 2023; revised 13 April 2023; accepted 1 August 2023

Abstract:

In this study, we successfully synthesized europium-doped TiO_2 (TiO_2:Eu^{3+}) nanomaterials (NMs) with crystalline sizes ranging from 6.5 to 71.7 nm through a sol-gel method. Analysis of X-ray diffraction (XRD) patterns and ultraviolet-visible (UV-Vis) spectra indicates that the substitution of smaller-sized Ti^{4+} ions (0.745 Å) by larger-sized Eu^{3+} ions (0.947 Å) was more efficient at higher doping concentrations and annealing temperatures. Photoluminescence (PL) and photoluminescence excitation (PLE) spectra of the synthesized TiO_2:7%Eu^{3+} NMs exhibit a strong red emission band peaking at 613 nm and remarkable absorption in the blue light region centered at 463 nm, making them suitable for use in white light-emitting diode (WLED) applications. Our findings reveal that both annealing temperature and doping concentration significantly influence the structure and properties of these materials. Besides, the research team has seen, under the experimental conditions, the TiO_2:7%Eu^{3+} sample annealed at 800°C exhibits the highest PL intensity. These results underscore the potential of the synthesized TiO_2:Eu^{3+} NMs as red-emitting materials for WLED applications.

Keywords: **Eu^{3+} doped TiO_2, nanomaterials (NMs), photoluminescence, sol-gel method, TiO_2.**

Classification numbers: **2.1, 2.3**

1. Introduction

In the present era, the realization of WLEDs can be achieved through three distinct techniques, namely: i) the combination of red, green, and blue LED chips; ii) the utilization of near-ultraviolet (NUV) LED chips in conjunction with tricolor phosphors (blue, green, and red phosphors); iii) the employment of a yellow-emitting $Y_3Al_5O_{12}$:Ce^{3+} phosphor with a blue LED chip [1]. Nonetheless, current commercial WLEDs frequently suffer from a deficiency in the red light spectrum, resulting in a low color rendering index (CRI<80) [2]. Consequently, the incorporation of a red light emission component into WLEDs becomes imperative for achieving high CRI values. To address this challenge, the development of red-emitting phosphors that can be efficiently excited by blue or near-NUV light has become a pressing need [1-3]. Unfortunately, existing red-emitting nitride or sulfide-based materials, which are excitable by blue or NUV light, are marred by chemical instability and environmental hazards [4, 5]. Recent research efforts have thus focused on red-emitting Eu^{3+}-doped oxide phosphors that can be excited by NUV light, such as Y_2O_3, $CaMoO_4$ [6, 7]. Amongst semiconductor oxides, anatase-phase titanium dioxide (TiO_2) emerges

*Corresponding author: Email: trituan@ctu.edu.vn

as a promising host lattice due to its attributes of a high band gap (3.2 eV), chemical stability, facile synthesis, affordability, non-toxicity, and non-hygroscopic behavior [2]. Recent studies have demonstrated that Eu^{3+}-doped TiO_2 can be effectively excited by blue light and exhibit a red emission band spanning from 540 to 740 nm, attributed to the $^5D_0$-^7F_j (j=1-4) transitions of Eu^{3+} ions [1, 8]. However, optimizing the procedure for synthesizing Eu^{3+}-doped TiO_2 phosphors remains challenging owing to the significant differences in ionic radius and charge imbalance [2].

This study presents successful doping of Eu^{3+} ions into the TiO_2 host lattice using a sol-gel method. It comprehensively investigates and discusses the impact of annealing temperature and doping concentration on the structure and optical properties of Eu^{3+}-doped TiO_2 NMs.

2. Materials and methods

2.1. Synthesis of Eu^{3+} doped TiO_2 NMs

Eu^{3+}-doped TiO_2 (TiO_2:x%Eu^{3+}, x=1-10) NMs were synthesized via a sol-gel method. Initially, a mixture of $Eu(NO_3)_3$ and 20 ml of ethanol was stirred for 30 minutes. Subsequently, 5 ml of titanium butoxide ($Ti(OBu)_4$) and 0.85 ml of acetic acid (CH_3COOH) were added and stirred continuously for 10 minutes. Nitric acid (HNO_3) was gradually introduced to maintain a pH of 2 in the solution. It is worth noting that the calculated mole ratio of Eu^{3+} ions in TiO_2 ranged from 1 to 10 mol%. In the subsequent step, the solution was further stirred for 2 hours and then air-dried at room temperature for 24 hours to yield a dry gel product. Finally, this dry gel was subjected to annealing at 100°C for 12 hours, followed by a second annealing process in air, ranging from 200 to 1000°C for 2 hours, to obtain the TiO_2:Eu^{3+} NMs.

2.2. Characterisation

The surface morphology and crystallite structure of TiO_2:Eu^{3+} NMs were analyzed using a field emission scanning electron microscope (FESEM-JEOL JSM-7600F) and XRD, D8 Advanced). The band gap energy was determined through UV-Vis absorption spectra, employing the JASCO V-750 Spectrophotometer. PL and PLE spectra were recorded using a Nanolog spectrophotometer, excited by a 450 W Xenon lamp, at room temperature.

3. Results and discussion

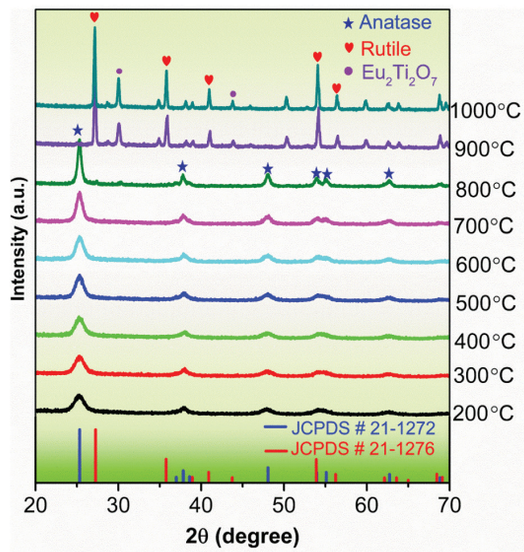

Fig. 1. XRD patterns of as-synthesized TiO_2:7%Eu^{3+} NMs annealed in air at different temperatures of 200-1000°C for 2 hours.

The XRD patterns of the as-synthesized TiO_2:7%Eu^{3+} NMs, annealed in air in the range of 200-1000°C for 2 hours, are presented in Fig. 1. At the lower temperature of 700°C, distinct diffraction peaks are observed at 2θ=25.28, 37.88, 48.09°, 53.98, 55.20, and 62.69°, corresponding to the (101), (004), (200), (105), (211), and (204) planes of the TiO_2 anatase phase (JCPDS # 21-1272), without any evidence of impurity phases [1]. When the temperature [8] is raised to 800°C, in addition to the anatase phase, new diffraction peaks attributed to rutile (JCPDS # 21-1276) [9] and Eu_2TiO_7 (JCPDS 01-087-1852) phases emerge in the XRD pattern. These peaks become prominent in samples annealed at higher temperatures (900 and 1000°C), indicating a phase transition from anatase to TiO_2 rutile and Eu_2TiO_7 at 800°C.

Figure 2 presents the focused XRD patterns within the 2θ range of 20 to 45°, revealing an increase in peak intensity and a reduction in the full width at half maximum (FWHM) with increasing temperature. This observation confirms the formation of a more well-defined crystalline structure with higher annealing temperatures. Furthermore, a slight shift in the peak position towards a larger angle at higher temperatures is noted. This shift can be attributed to the enhanced substitution of smaller-sized Ti^{4+} ions (0.745 Å) by larger-sized Eu^{3+} ions (0.947 Å) within the TiO_2 host lattice [10, 11].

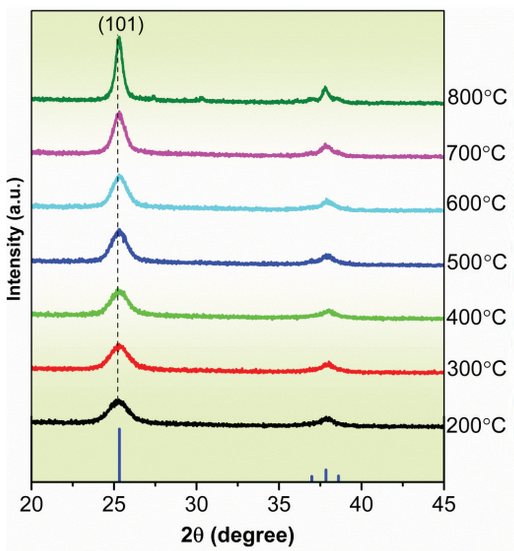

Fig. 2. XRD patterns focused in 2θ range from 20 to 45° of as-synthesized TiO_2:7%Eu^{3+} NMs annealed in air in the range of 200-800°C for 2 hours.

Moreover, the average crystallite size of all samples was determined using Debye-Scherrer's Eq. (1) based on the FWHM of the (101) peak [12]:

$$D = \frac{K\lambda}{\beta\cos\theta} \text{ (nm)} \quad (1)$$

where λ=1.54 Å, β, θ and K=0.9 are the X-ray wavelength, full width at half maximum of a diffraction peak, diffraction angle, and Scherrer constant, respectively. The calculated results are listed in Table 1, indicating a gradual increase in average crystallite size ranging from 6.5 Å to 71.7 Å with an increase in annealing temperature from 200 to 1000°C. A similar trend has also been reported in a previous study [12].

Table 1. An average crystalite size of TiO_2:7%Eu^{3+} NMs calculated at the (101) plane.

Temperature (°C)	β (degree)	2θ (degree)	~D (nm)
As-synthesize TiO_2:7%Eu^{3+}	1.22	25.3	6.5
200	1.22	25.3	6.5
300	1.19	25.3	6.7
400	1.17	25.3	6.8
500	1.03	25.3	7.7
600	0.93	25.3	8.6
700	0.80	25.4	10.0
800	0.43	25.4	18.5
900	0.30	27.2	51.3
1000	0.21	27.2	71.7

Figure 3 illustrates XRD patterns of TiO_2:x%Eu^{3+} (x=0-10) NMs annealed in air at 800°C for 2 hours. Notably, only diffraction peaks corresponding to the TiO_2 anatase phase (JCPDS # 21-1272) were detected [1]. Additionally, the XRD patterns reveal a decrease in peak intensity with an increase in the concentration of doped Eu^{3+} ions, suggesting that higher doping concentrations result in reduced crystallinity of TiO_2. This phenomenon can be attributed to the presence of Eu^{3+} ions, which may impede the phase transition process in TiO_2 materials. Furthermore, the peak position exhibits a slight shift towards larger angles with higher doping concentrations, which can be attributed to the enhanced substitution of smaller-sized Ti^{4+} ions (0.745 Å) by larger-sized Eu^{3+} ions (0.947 Å) within the TiO_2 lattice [2].

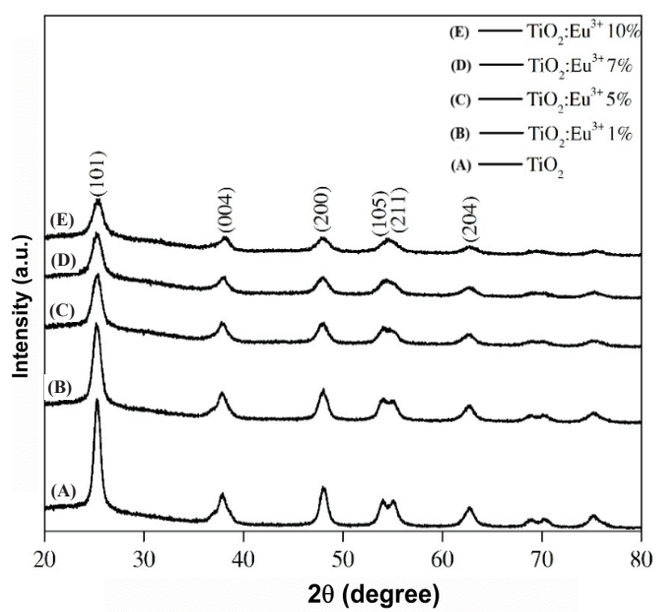

Fig. 3. XRD patterns of TiO_2:*x*%Eu^{3+} (x=0-10) NMs annealed in air at 800°C for 2 hours.

Figure 4 presents field emission scanning electron microscope (FESEM) images of TiO_2:7%Eu^{3+} NMs annealed in air at different temperatures ranging from 200 to 1000°C for 2 hours. The observations indicate a gradual increase in particle size with rising annealing temperature. This phenomenon is likely caused by the agglomeration of small clusters, resulting in the formation of larger particles at elevated temperatures [13]. The largest particle size from 200 nm at 200°C to 1 µm was obtained at 1000°C.

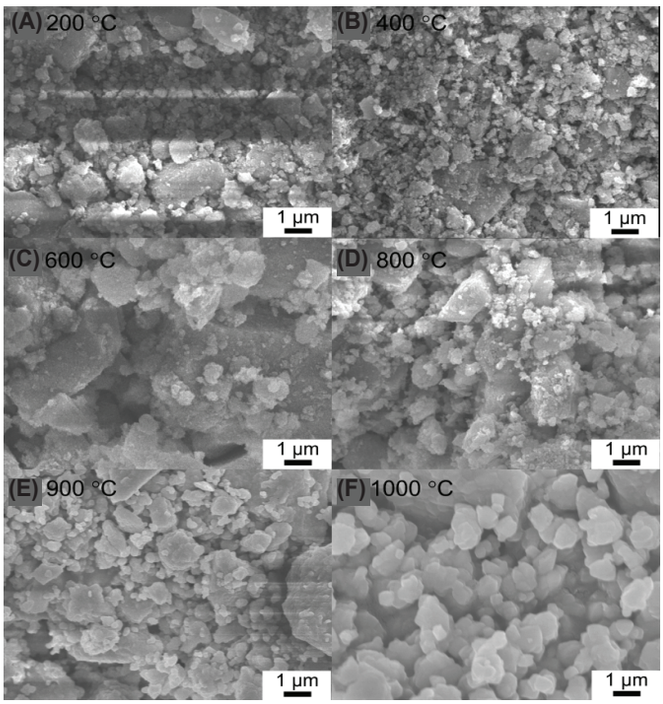

Fig. 4. FESEM images of TiO_2:7%Eu^{3+} NMs annealed in air at different temperatures ranging from 200-1000°C for 2 hours (A-F).

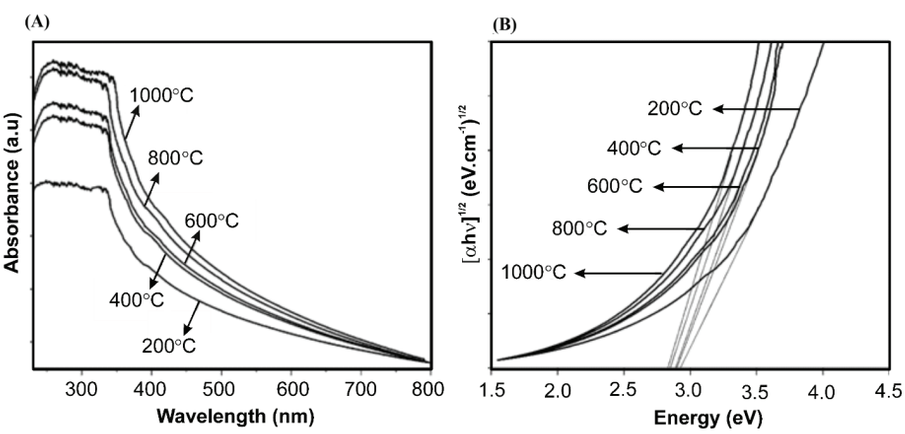

Fig. 5. UV-Vis absorption spectra of TiO_2:7%Eu^{3+} NMs annealed at 200, 400, 600, 800, and 1000°C (A), relationship between hν and $(\alpha h\nu)^2$ (B).

Figure 5A displays the UV-Vis spectra of TiO_2:7%Eu^{3+} NMs annealed in air at various temperatures within the range of 200 to 1000°C for 2 hours. It is evident that TiO_2:7%Eu^{3+} NMs exhibit strong absorption in the ultraviolet region (200-350 nm) and a weaker absorbance band in the NUV to visible range (350-500 nm). The former is attributed to the near band-edge absorption of TiO_2, while the latter is likely associated with the presence of Eu^{3+} ions doped into the TiO_2 lattice [3]. Furthermore, an increase in absorption intensity with rising annealing temperature can be attributed to the substitution of larger-sized Eu^{3+} ions for smaller Ti^{4+} ions. This phenomenon is also supported by the XRD pattern analysis presented in Fig. 2. The bandgap energy (E_g) of TiO_2:Eu^{3+} NMs can be estimated from the absorption spectra in Fig. 5A using the Tauc Eq. (2) [1-3]:

$$(\alpha h\nu)^{1/n} = K(h\nu - E_g) \quad (2)$$

where α, hν, K are the absorption coefficient, photon energy and characteristic constant of the specific material, respectively. For an indirect semiconductor like TiO_2, n=2. Utilising the Tauc Eq. (2), the E_g values for TiO_2:7%Eu^{3+} NMs annealed at 200, 400, 600, 800, and 1000°C were calculated to be 2.94, 2.90, 2.89, 2.85, and 2.82 eV, respectively. These values indicate that the bandgap of TiO_2:7%Eu^{3+} NMs is smaller than that of pure TiO_2 (E_g=3.2 eV) and gradually decreases with higher annealing temperatures [4, 5, 14]. This phenomenon can be attributed to the increased substitution of smaller-sized Ti^{4+} ions with larger-sized Eu^{3+} ions within the TiO_2 lattice, consistent with findings reported in recent studies [1-3].

It has been reported that the incorporation of Eu^{3+} ions into the TiO_2 lattice introduces intermediate energy levels located below the conduction band, resulting in the narrowing of the energy band gap of TiO_2 [Ceramics International 43 (2017) 9838-9845]. Conversely, when Eu^{3+} is introduced into the host lattice of TiO_2, it can increase the density of absorption centers, subsequently leading to higher absorbance in the UV-Vis spectrum. Therefore, a higher substitution of larger-sized Eu^{3+} ions can increase the density of absorption centers, resulting in enhanced absorption.

Figure 6 presents the PLE spectrum measured at 613 nm (A) and the PL spectrum excited at 463 nm (B) of the TiO_2:7%Eu^{3+} NMs annealed in air at 800°C for 2 hours. The PL spectrum exhibits a red emission band spanning from 540 to 740 nm, with peak wavelengths at 577, 594, 613, 655, and 703 nm. These peaks correspond to the $^5D_0$-$^7F_0$, $^5D_0$-$^7F_1$, $^5D_0$-$^7F_2$, $^5D_0$-$^7F_3$, and $^5D_0$-$^7F_4$ transitions of Eu^{3+} ions, respectively [2, 4, 15-17]. As depicted in Fig. 6B, the PLE spectrum displays notable absorption in the blue light region centred at 463 nm, which is well explained by a $^7F_0$-$^5D_2$ transition of Eu^{3+} ions [2, 5].

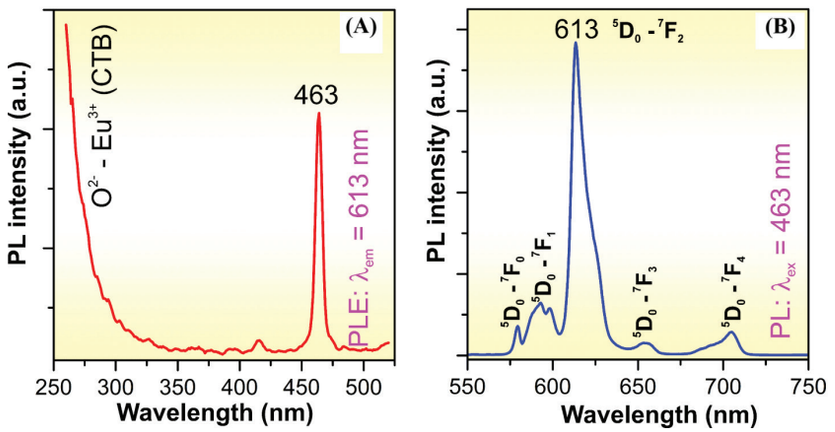

Fig. 6. PLE spectrum measured at 613 nm (A) and PL spectrum excited at 463 nm (B) of the TiO_2:7%Eu^{3+} NMs annealed in air at 800°C for 2 hours.

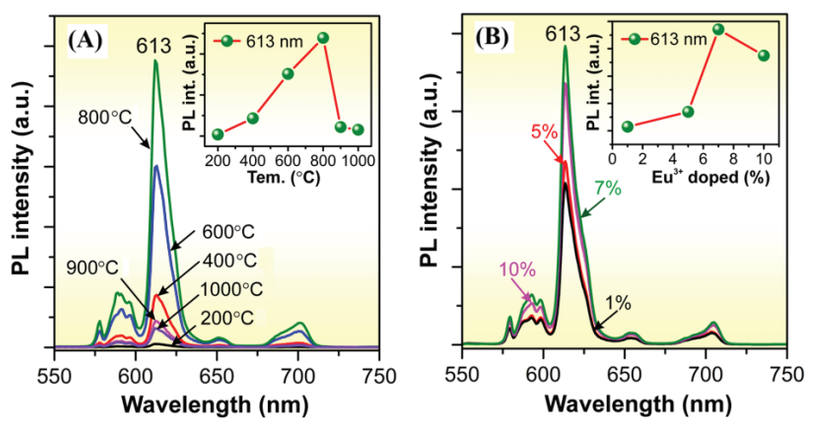

Fig. 7. PL spectra of TiO_2:7%Eu^{3+} NMs annealed in air at different temperatures ranging from 200-1000°C for 2 hours (A) and TiO_2:x%Eu^{3+} (x=0-10) NMs annealed in air at 800°C for 2 hours (B).

Figure 7A presents the PL spectra excited at 463 nm of TiO_2:7%Eu^{3+} NMs annealed in air at different temperatures within the range of 200 to 1000°C for 2 hours. All PL spectra exhibit a similar shape, but their intensities are significantly dependent on the annealing temperature. As the annealing temperature increases from 200 to 800°C, there is a gradual enhancement in PL intensity. This improvement can be attributed to the formation of a more well-defined crystalline structure or the substitution of larger-sized Eu^{3+} ions for smaller-sized Ti^{4+} ions within the TiO_2 host lattice [13, 18, 19]. However, after reaching 800°C, there is a marked reduction in PL intensity, which can be attributed to the phase transition from anatase to rutile or the formation of the Eu_2TiO_7 compound.

Figure 7B illustrates the PL spectra of TiO_2:x%Eu^{3+} (x=0-10) NMs annealed in air at 800°C for 2 hours. While the shape of the spectra remains consistent, there is a significant variation in PL intensity with increasing Eu^{3+} ion concentration. The PL intensity gradually increases within the range of Eu^{3+} ion concentrations from 1 to 7%, and then decreases at a higher concentration of 10%. This phenomenon can be explained by PL quenching due to concentration effects [5, 15, 20]. At low doping concentrations, the Eu^{3+} ions are widely spaced apart, resulting in a low density of luminescent centres and, consequently, a low luminescent intensity. Conversely, at high concentrations, the proximity of Eu^{3+} ions reaches a threshold where energy transfer among the Eu^{3+} ions is facilitated, leading to a decrease in PL intensity (as seen in Fig. 7B). This is known as the PL quenching phenomenon. In this study, the PL quenching effect is observed at a higher Eu^{3+} doping concentration of 7%. Thus, the optimal concentration of Eu^{3+} ions to achieve the highest PL intensity is determined to be 7%.

4. Conclusions

In summary, we have successfully synthesised red-emitting Eu^{3+}-doped TiO_2 NMs (NMs) through a sol-gel method. Our study highlights the significant influence of annealing temperature and doping concentration on the crystalline structure and optical properties of TiO_2:Eu^{3+} NMs. Notably, annealing at 800°C facilitated a phase transition from the anatase phase to a combination of TiO_2 rutile and Eu_2TiO_7 phases. Furthermore, a gradual increase in annealing temperature within the range of 200 to 1000°C led to a more pronounced substitution of smaller-sized Ti^{4+} ions (0.745 Å) by larger-sized Eu^{3+} ions (0.947 Å) within the TiO_2 lattice. The PL spectra, excited at 463 nm, exhibited a substantial red emission band with peak wavelengths at 577, 594, 613, 655, and 703 nm, corresponding to the $^5D_0$-$^7F_0$, $^5D_0$-$^7F_1$, $^5D_0$-$^7F_2$, $^5D_0$-$^7F_3$, and $^5D_0$-$^7F_4$ transitions of Eu^{3+} ions, respectively. Remarkably, the TiO_2:7%Eu^{3+} sample annealed at 800°C demonstrated the highest PL intensity, indicating the optimal conditions for emission enhancement. In conclusion, our study underscores the promising potential of TiO_2:Eu^{3+} NMs for applications in WLEDs, owing to their unique optical properties and tunability.

CRediT author statement

Nguyen Tri Tuan: Reviewing, Methodology, Formal analysis, Writing, Editing; Tong Thi Hao Tam, Nguyen Tu, Do Quang Trung, Nguyen Van Du, Tran Minh Tien, Vu Thi Hang: Data analysis; Nguyen Trong Tuan, Nguyen Van Quang: Editing; Manh Trung Tran: Reviewing, Editing.

ACKNOWLEDGEMENTS

This research is funded by the Vietnam National Foundation for Science and Technology Development (NAFOSTED) under grant number 103.03-2017.375.

COMPETING INTERESTS

The authors declare that there is no conflict of interest regarding the publication of this article.

REFERENCES

[1] W. Chen, A. Zhou, X. Yang, et al. (2013), "Structure and luminescence properties of TiO_2:Eu^{3+} for WLED", *J. Alloys Compd.*, **581**, pp.330-334, DOI: 10.1016/j.jallcom.2013.07.072.

[2] A.K. Kunti, S.K. Sharma (2017), "Structural and spectral properties of red light emitting Eu^{3+} activated TiO_2 nanophosphor for white LED application", *Ceram. Int.*, **43(13)**, pp.9838-9845, DOI: 10.1016/j.ceramint.2017.04.166.

[3] M. Pal, U. Pal, J.M.G.Y. Jimenez, et al. (2012), "Effects of crystallisation and dopant concentration on the emission behavior of TiO_2:Eu nanophosphors", *Nanoscale Res. Lett.*, **7(1)**, pp.1-12, DOI: 10.1186/1556-276X-7-1.

[4] S. Stojadinovic, N. Radic, B. Grbic, et al. (2016), "Structural, photoluminescent and photocatalytic properties of TiO_2:Eu^{3+} coatings formed by plasma electrolytic oxidation", *Appl. Surf. Sci.*, **370**, pp.218-228, DOI: 10.1016/j.apsusc.2016.02.131.

[5] D. Komaraiah, E. Radha, J. James, et al. (2019), "Effect of particle size and dopant concentration on the Raman and the photoluminescence spectra of TiO_2:Eu^{3+} nanophosphor thin films", *J. Lumin.,* **211**, pp.320-333, DOI: 10.1016/j.jlumin.2019.03.050.

[6] N.D.Q. Anh, H.Y. Lee, T.T. Phuong, et al. (2017), "Y_2O_3:Eu^{3+} phosphor: A novel solution for an increase in color rendering index of multi-chip white LED packages", *J. Chinese Inst. Eng. Trans. Chinese Inst. Eng. A.*, **40(3)**, pp.228-234, DOI: 10.1080/02533839.2017.1299592.

[7] E. Red, C. Bi, S. Yan, et al. (2007), "Enhanced red emission in $CaMoO_4$:Bi^{3+}, Eu^{3+}", *J. Phys. Chem. C*, **111(35)**, pp.13256-13260, DOI: 10.1021/jp073991c.

[8] X. Xu, S. Wen, Q. Mao, et al. (2018), "N-Anchoring in rare earth-doped amorphous TiO_2 as a route to broadband down-conversion phosphor", *ACS Appl. Mater. Interfaces*, **10(45)**, pp.39238-39244, DOI: 10.1021/acsami.8b11998.

[9] D. Padayachee, A.S. Mahomed, S. Singh, et al. (2020), "Effect of the TiO_2 anatase/rutile ratio and Interface for the oxidative activation of n-Octane", *ACS Catal.*, **10(3)**, pp.2211-2220, DOI: 10.1021/acscatal.9b04004.

[10] O. Örnek, Z.A. Kösemen, S. Öztürk, et al. (2017), "Performance enhancement of inverted type organic solar cells by using Eu doped TiO_2 thin film performance enhancement of inverted type organic solar cells by using Eu doped TiO_2 thin film", *Surfaces and Interfaces*, **9**, pp.64-69, DOI: 10.1016/j.surfin.2017.08.003.

[11] Z. Rao, X. Xie, X. Wang, et al. (2019), "Defect chemistry of Er^{3+}-doped TiO_2 and its photocatalytic activity for the degradation of flowing gas-phase VOCs", *J. Phys. Chem. C.*, **123(19)**, pp.12321-12334, DOI: 10.1021/acs.jpcc.9b02093.

[12] X. Xue, R.L. Penn, E.R. Leite, et al. (2014), "Crystal growth by oriented attachment: Kinetic models and control factors", *Cryst. Eng. Comm.*, **16(8)**, DOI: 10.1039/c3ce42129e.

[13] N.V. Quang, N.T. Huyen, N. Tu, et al. (2021), "A high quantum efficiency plant growth LED by using a deep-red-emitting α-Al_2O_3:Cr^{3+} phosphor", *Dalt. Trans.*, **50(36)**, pp.12570-12582, DOI: 10.1039/d1dt00115a.

[14] M. Fhoula, T. Kallel, M. Messaoud, et al. (2019), "Morphological, spectroscopic and photocatalytic properties of Eu^{3+}:TiO_2 synthesised by solid-state and hydrothermal-assisted sol-gel processes", *Ceram. Int.*, **45(3)**, pp.3675-3679, DOI: 10.1016/j.ceramint.2018.11.029.

[15] B. Kee, I. Kwon, H. Kyoung, et al. (2008), "Spectroscopy of nanocrystalline TiO_2:Eu^{3+} phosphors", *Colloids and Surfaces A: Physicochemical and Engineering Aspects*, **313-314**, pp.82-86, DOI: 10.1016/j.colsurfa.2007.04.075.

[16] B. Mili, K. Vukovi, G. Dra (2017), "Effects of Li^+co-doping on properties of Eu^{3+} activated TiO_2 anatase nanoparticles", *Optical. Materials*, **72**, pp.316-322, DOI: 10.1016/j.optmat.2017.06.029.

[17] S. Culubrk, J.M. Nedeljkovi (2014), "Sensors and actuators B : Chemical temperature sensing with Eu^{3+} doped TiO_2 nanoparticles", *Sensors and Actuators B: Chemical*, **201**, pp.46-50, DOI: 10.1016/j.snb.2014.04.108.

[18] N.T. Huyen, N. Tu, N.V Quang, et al. (2022), "Excellent quantum efficiency and superior color purity red-emitting $CaAl_{12}O_{19}$-$CaAl_4O_7$-$MgAl_2O_4$:Mn^{4+} phosphors for plant growth and high color rendering index white light-emitting diode applications", *ACS Appl. Electron. Mater.*, **4(9)**, pp.4322-4331, DOI: 10.1021/acsaelm.2c00603.

[19] M.T. Tran, N. Tu, N.V. Quang, et al. (2021), "Excellent thermal stability and high quantum efficiency orange-red-emitting $AlPO_4$:Eu^{3+} phosphors for WLED application", *J. Alloys Compd.*, **853**, DOI: 10.1016/j.jallcom.2020.156941.

[20] H. Li, Y. Sheng, H. Zhang, et al. (2011), "Synthesis and luminescent properties of TiO_2:Eu^{3+} nanotubes", *Powder Tech.*, **212(2)**, pp.372-377, DOI: 10.1016/j.powtec.2011.06.019.